ISSN 0001-4338, Izvestiya, Atmospheric and Oceanic Physics, 2012, Vol. 48, No. 5, pp. 528–537. © Pleiades Publishing, Ltd., 2012.
Original Russian Text © E.V. Ezhova, Yu.I. Troitskaya, 2012, published in Izvestiya AN. Fizika Atmosfery i Okeana, 2012, Vol. 48, No. 5, pp. 591–601.

Nonstationary Dynamics of Turbulent Axisymmetric Jets in a Stratified Fluid: Part 2. Mechanism of Excitation of Axisymmetric Oscillations in a Submerged Jet[1]

E. V. Ezhova and Yu. I. Troitskaya

Institute of Applied Physics, Russian Academy of Sciences, ul. Ul'yanova 46, Nizhni Novgorod, 603950, Russia
e-mail: ezhova@hydro.appl.sci-nnov.ru

Received April 12, 2011

Abstract—It was shown based on laboratory experiments in a Large Thermally Stratified Tank (LTST) at the Institute of Applied Physics of the Russian Academy of Sciences that a turbulent axisymmetric jet in a stratified fluid with a sharp density drop (a pycnocline) intensively generates internal waves. An axisymmetric oscillation mode, for which a sufficient condition of stability in the parallel flow approximation is met, served as their source. This paper studies the stability of a nonparallel flow (with self-similar velocity profiles) that simulates a jet flow in the lower part of the pycnocline with respect to the axisymmetric mode. The estimates of the axisymmetric mode near the pycnocline are in agreement with the experimental data. The signs of the self-oscillating mode of the jet were experimentally revealed and the possibility of self-oscillations was theoretically proved: it was shown that the flow in the pycnocline vicinity is absolutely unstable.

Keywords: turbulent jets, axisymmetric mode, nonparallel jets, stratification, absolute instability.

DOI: 10.1134/S0001433812050027

INTRODUCTION

The hydrodynamic instability of jet flows from a steady source is the key reason for their nonstationary modes. It was found that two lower oscillation modes predominate on a jet with a circular cross section, namely an axisymmetric (varicose) mode and a spiral (helical) one [1–3]. The authors of [4–7] theoretically proved and experimentally verified that the axisymmetric mode is the most unstable (when compared to other modes) near the outlet, where the thickness of the shear layer of the jet flow is smaller than its radius. On the contrary, the theory of the hydrodynamic instability of plane-parallel jet flows with the velocity profiles simulating the flow in a jet at a large distance from the source shows that the helical mode is unstable [8]. This conclusion was verified by an experiment where the jet was subjected to a periodic external action. However, a number of experiments [9–12] show that the spiral mode is not always predominant: axisymmetric coherent structures are observed along with the spiral mode at large distances from the source.

Such peculiarities of jet flows were observed in the experiments on studying the nonstationary dynamics of turbulent forced jets in a stratified fluid described in Section 1 of [13]. The experiments were staged in the Large Thermally Stratified Tank (LTST) at the Institute of Applied Physics of the Russian Academy of Sciences. A jet with a density equal to the density of the lower stratification layer escaped a hole with the circular cross section upright with an initial pulse. In this case, a fountain (a jet with negative buoyancy and a nonzero vertical pulse) was formed in the thermocline region. The fountain dynamics was studied using underwater video recording. Data processing pointed to the predominant excitation of an axisymmetric mode of the fountain, leading to the intensive generation of internal waves. The necessary condition for the instability of a jet with a circular cross section with respect to an axisymmetric perturbation is an analog of the Rayleigh criterion for the instability of plane-parallel flows:

$$\frac{d}{dr}\left(\frac{U_0'}{r}\right) = 0,$$

where $U_0(r)$ is the profile of the average longitudinal velocity in the jet. The measurements described in Section 1 showed that the instability criterion is not met for the jet observed in the experiment; however, an axisymmetric mode is excited on it.

Real jet flows are nonparallel; however, as a rule, this fact does not play any important role for different

[1] E. V. Ezhova, D. A. Sergeev, A. A. Kandaurov, et al., "Nonstationary Dynamics of Submerged Turbulent Axisymmetric Jets in a Stratified Fluid. Part 1: Experimental Study," Izv., Atmos. Ocean. Phys. **48** (4), 461–470 (2009).

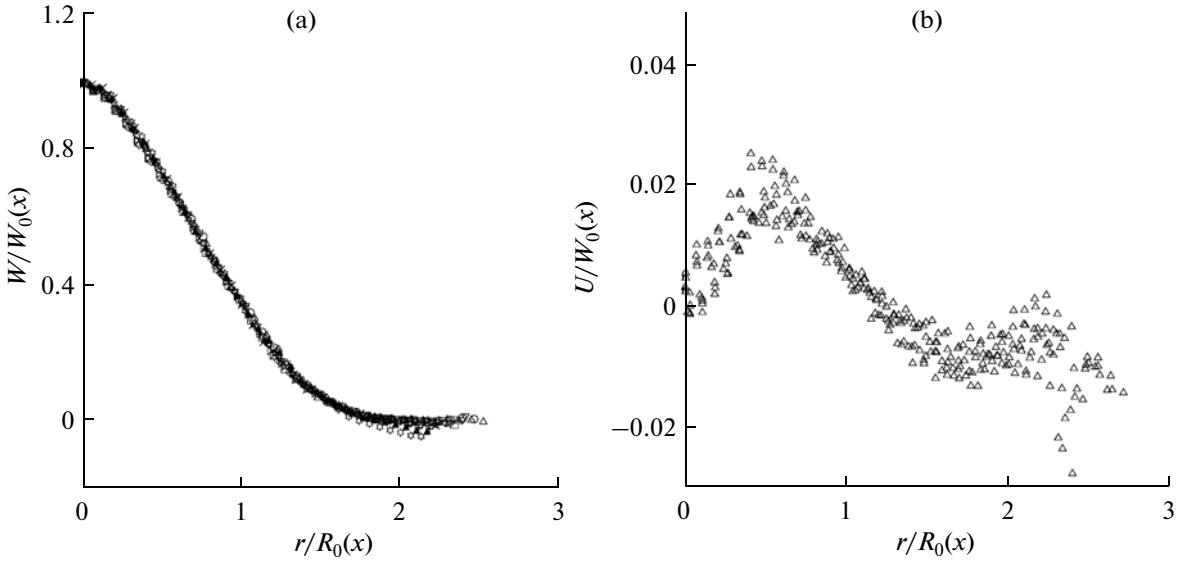

Fig. 1. Normalized profiles of the average longitudinal (left) and transverse (right) velocity.

applications, since the radial velocity of the flow turns out to be small as compared to the longitudinal one [14]. Nevertheless, the nonparallelism of the flow turns out to be the factor that determines the stability of an axisymmetric mode. For example, the authors of [15] studied the spatial instability of a submerged Landau jet whose radius increases downstream and showed that the axisymmetric mode became unstable. The jet with a circular cross section considered in this paper is also nonparallel, and one can expect the development of an axisymmetric mode in it. This section considers the temporal instability of the axisymmetric mode of a nonparallel flow with self-similar velocity profiles, estimates the frequency of this mode near the thermocline, and compares it with the frequency of internal waves measured in the experiment.

The experiment described in Section 1 showed that the jet oscillation spectrum always has a pronounced maximum that corresponds to an axisymmetric mode, while a spiral mode predominates in the experiments for studying the instability of turbulent jets in a homogeneous fluid at some distance from the source. This peculiarity can be related to the development of a self-oscillation regime of a varicose mode on the flow with a counterflow generated in a ring-shaped region around the main flow in the thermocline. It was shown in [16, 17] that a counterflow in plane-parallel and weakly nonparallel flows can lead to the development of absolute instability and self-oscillations. This paper discusses the possibility of the development of a self-oscillation regime of an axisymmetric mode in a nonparallel jet in the vicinity of a thermocline.

The paper is structured as follows. Section 1 gives an approximation of the average jet flow observed in the experiment of [13]. Section 2 studies its stability in the approximation suggested in [15, 18, 19]. Section 3 discusses the conditions for the development of absolute instability in a jet.

1. APPROXIMATION OF THE AVERAGE VELOCITY PROFILE OF THE JET FLOW

To obtain average velocity profiles in a jet, the instantaneous fields of the longitudinal and transverse velocity calculated from experimental data were averaged over the video recording time (20 min) [13]. Each profile of the longitudinal and transverse velocity was normalized to the maximal longitudinal velocity W_0 and the lateral scale R_0, which was determined by an e-fold decrease in the maximum transverse velocity. A family of normalized profiles is shown in Fig. 1. The average profiles of the longitudinal velocity before the jet entrance to the thermocline have a typical bell-like shape, and a counterflow is formed in the thermocline region. The average radial velocity is positive inside the jet; i.e., an outflow of the fluid from the jet axis yielding its expansion is observed, while beyond the jet the velocity is negative, which corresponds to the turbulent entrainment of the fluid.

The dependences of R_0 and W_0 on the coordinate along the jet are shown in Fig. 2. They are well approximated with self-similar dependences $R_0 = \varepsilon x$ ($\varepsilon = 0.1$), $W_0 = \beta/x$ ($\beta = 600$ cm^2/s for the experiment with an output velocity of 150 cm/s; $\beta = 554$ cm^2/s for the experiment with an output velocity of 110 cm/s). Thus,

$$U = \frac{\beta}{x} F_1\left(\frac{r}{\varepsilon x}\right), \quad W = \frac{\beta}{x} F_2\left(\frac{r}{\varepsilon x}\right). \tag{1}$$

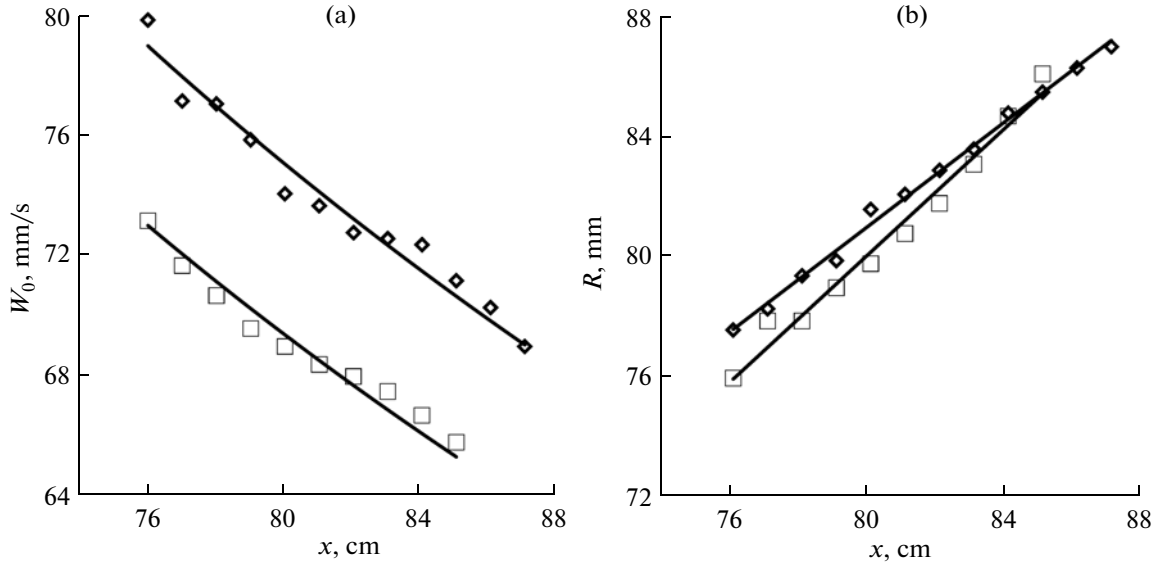

Fig. 2. Diagonal scale (right) and the maximum longitudinal velocity (left) of the jet as a function of the distance along it for experiments with the velocities of the fluid outflow from holes of 110 and 150 cm/s.

Let us introduce the self-similar coordinate $\xi = \frac{r}{x}$. The profile of the longitudinal velocity was approximated using an exponential function of the type

$$F_2(\xi) = \exp(-\xi^2/\varepsilon^2). \quad (2)$$

To determine the radial velocity profile corresponding to such transverse velocity profile, we consider the equation of continuity in cylindrical coordinates:

$$\frac{\partial U}{\partial r} + \frac{U}{r} + \frac{\partial W}{\partial x} = 0. \quad (3)$$

Let us substitute the self-similar solution of type (2) into Eq. (3) and turn to self-similar variables $\left(\xi = \frac{r}{x}, x\right)$. Then, Eq. (3) will take the form

$$\frac{1}{\xi}\frac{d}{d\xi}(\xi F_1) = \frac{d}{d\xi}(\xi F_2). \quad (4)$$

Substituting the function approximating longitudinal velocity profile (2), into Eq. (4) and taking into account condition $\xi F_1|_{\xi=0} = 0$, we obtain

$$F_1(\xi) = \frac{\varepsilon}{\xi}\left\{\varepsilon\left(\frac{1}{2} + \frac{\xi^2}{\varepsilon^2}\right)\exp\left(-\frac{\xi^2}{\varepsilon^2}\right) - \frac{\varepsilon}{2}\right\}. \quad (5)$$

The average longitudinal velocity profiles approximated by the exponential function are shown in Fig. 3. It can be seen from the figure that the exponential function adequately approximates the experimental profiles of the turbulent jet velocity.

2. CALCULATION OF THE STABILITY OF THE AXISYMMETRIC MODE OF A NONPARALLEL FLOW

To investigate the stability of the velocity profile specified by function (2), we use equation of continuity (3) and turn to the vorticity and the stream function variables:

$$\frac{\partial \psi}{\partial x} = ru, \quad \frac{\partial \psi}{\partial r} = -rw, \quad \Omega = \frac{\partial u}{\partial x} - \frac{\partial w}{\partial r}. \quad (6)$$

Let us consider the set of equations of hydrodynamics of a viscous incompressible fluid in cylindrical coordinates:

$$\frac{\partial \Omega}{\partial t} + \frac{\partial}{\partial r}\left(\frac{\Omega}{r}\frac{\partial \psi}{\partial x}\right) - \frac{1}{r}\frac{\partial}{\partial x}\left(\Omega\frac{\partial \psi}{\partial r}\right) = \nu\left(\frac{\partial^2 \Omega}{\partial x^2} + \frac{1}{r}\frac{\partial}{\partial r}\left(r\frac{\partial \Omega}{\partial r}\right) - \frac{\Omega}{r^2}\right), \quad (7)$$

$$\Omega = \frac{1}{r}\left(\frac{\partial^2 \psi}{\partial r^2} + \frac{\partial^2 \psi}{\partial x^2}\right) - \frac{1}{r^2}\frac{\partial \psi}{\partial r}. \quad (8)$$

A self-similar solution in the vorticity and stream function variables has the form

$$\psi = xf\left(\frac{r}{x}\right), \quad \Omega = \frac{1}{x^2}\chi\left(\frac{r}{x}\right). \quad (9)$$

Let us turn to the self-similar variables $\left(\xi = \frac{r}{x}, x\right)$, introduce the variable $\tau = \frac{\nu t}{x^2}$, as in [15, 18, 19] and

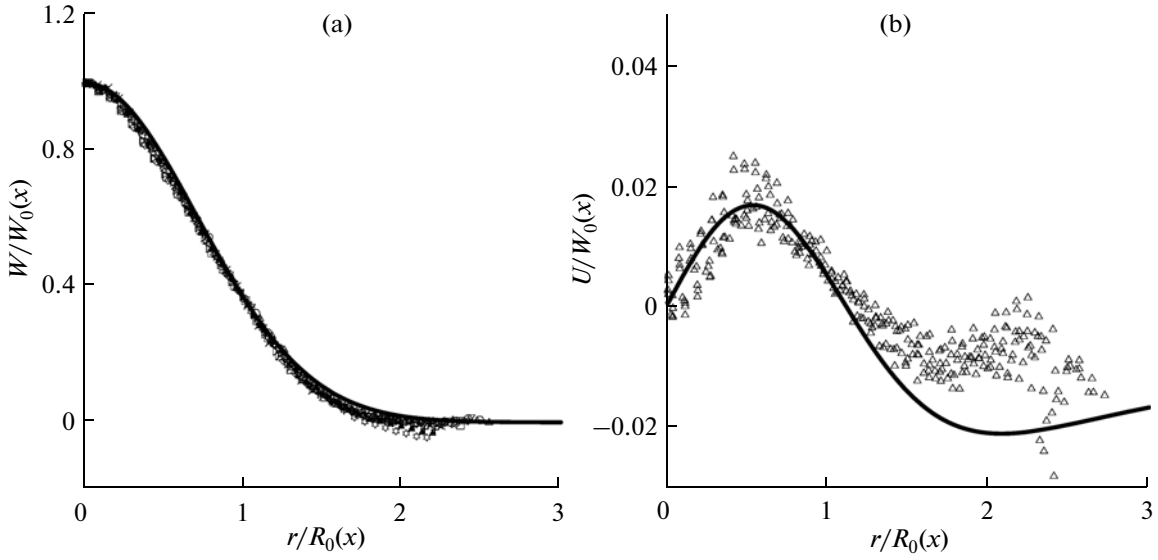

Fig. 3. Approximation of velocity components. The longitudinal velocity is on the left; the radial velocity is on the right.

search for the solution of nonstatonary equations (7)–(8) in the form

$$\psi(\xi,x,t)=xf\left(\xi,x,\tau=\frac{\nu t}{x^2}\right),$$
$$\Omega(\xi,x,t)=\frac{1}{x^2}\chi\left(\xi,x,\tau=\frac{\nu t}{x^2}\right). \tag{10}$$

Then, the set of equations for f and χ will take the form

$$\nu\frac{\partial\chi}{\partial\tau}+\frac{1}{\xi}\frac{\partial\chi}{\partial\xi}\left(f+x\frac{\partial f}{\partial x}-2\tau\frac{\partial f}{\partial\tau}\right)-\frac{\chi}{\xi^2}\left(f-\xi\frac{\partial f}{\partial\xi}+x\frac{\partial f}{\partial x}-2\tau\frac{\partial f}{\partial\tau}\right)$$
$$-\frac{1}{\xi}\frac{\partial f}{\partial\xi}\left(-2\chi+x\frac{\partial\chi}{\partial x}-2\tau\frac{\partial\chi}{\partial\tau}\right)$$
$$=\nu\left(6\chi-4x\frac{\partial\chi}{\partial x}+6\xi\frac{\partial\chi}{\partial\xi}-2x\xi\frac{\partial^2\chi}{\partial x\partial\xi}+\xi^2\frac{\partial^2\chi}{\partial\xi^2}+x^2\frac{\partial^2\chi}{\partial x^2}+4\tau\frac{\partial\chi}{\partial\tau}+4\tau^2\frac{\partial^2\chi}{\partial\tau^2}+\frac{\partial^2\chi}{\partial\xi^2}+\frac{1}{\xi}\frac{\partial\chi}{\partial\xi}-\frac{\chi}{\xi^2}\right), \tag{11}$$

$$\chi=\left(\frac{1}{\xi}+\xi\right)\frac{\partial^2 f}{\partial\xi^2}+\frac{2x}{\xi}\frac{\partial f}{\partial x}-2x\frac{\partial^2 f}{\partial x\partial\xi}+\frac{x^2}{\xi}\frac{\partial^2 f}{\partial x^2}+\frac{2\tau}{\xi}\frac{\partial f}{\partial\tau}+2\tau\frac{\partial^2 f}{\partial\tau\partial\xi}-\frac{2\tau x}{\xi}\frac{\partial^2 f}{\partial x\partial\tau}+\frac{4\tau^2}{\xi}\frac{\partial^2 f}{\partial\tau^2}-\frac{1}{\xi^2}\frac{\partial f}{\partial\xi}. \tag{12}$$

The fact that Eqs. (11) and (12) contain terms proportional to τ and τ^2 gives no way of studying stability using the method of normal modes. We use the approximation used in [15, 18, 19]: the problem is considered for $0<t<T$, where T is a finite time of flow evolution within the limits of applicability of linearized equations. Then, we have $0<\tau<\nu T/x^2$ and $\tau\to 0$ as $x\to\infty$. In this approximation, the terms proportional to τ and τ^2 in Eqs. (11) and (12) can be neglected. Then, we obtain the following set of equations:

$$\nu\frac{\partial\chi}{\partial\tau}+\frac{1}{\xi}\frac{\partial\chi}{\partial\xi}\left(f+x\frac{\partial f}{\partial x}\right)-\frac{\chi}{\xi^2}\left(f-\xi\frac{\partial f}{\partial\xi}+x\frac{\partial f}{\partial x}\right)$$
$$-\frac{1}{\xi}\frac{\partial f}{\partial\xi}\left(-2\chi+x\frac{\partial\chi}{\partial x}\right)+\nu\left(\frac{2}{\xi}\frac{\partial f}{\partial\tau}+2\frac{\partial^2 f}{\partial\tau\partial\xi}-\frac{2x}{\xi}\frac{\partial^2 f}{\partial\tau\partial x}\right)$$
$$=\nu\left(6\chi-4x\frac{\partial\chi}{\partial x}+6\xi\frac{\partial\chi}{\partial\xi}-2x\xi\frac{\partial^2\chi}{\partial x\partial\xi}+\xi^2\frac{\partial^2\chi}{\partial\xi^2}+x^2\frac{\partial^2\chi}{\partial x^2}+\frac{\partial^2\chi}{\partial\xi^2}+\frac{1}{\xi}\frac{\partial\chi}{\partial\xi}-\frac{\chi}{\xi^2}\right), \tag{13}$$

$$\chi=\left(\frac{1}{\xi}+\xi\right)\frac{\partial^2 f}{\partial\xi^2}+\frac{2x}{\xi}\frac{\partial f}{\partial x}-2x\frac{\partial^2 f}{\partial x\partial\xi}+\frac{x^2}{\xi}\frac{\partial^2 f}{\partial x^2}-\frac{1}{\xi^2}\frac{\partial f}{\partial\xi}. \tag{14}$$

Let us use the change of variables $z=\ln(x/x_0)$ and search for the solution to the set of Eqs. (13) and (14) in the form $\chi=\chi_0(\xi)+\varepsilon\tilde{\chi}(\xi,z,\tau)$, $f=f_0(\xi)+\varepsilon\tilde{f}(\xi,z,\tau)$.

In the linear approximation over ε, the set of Eqs. (13) and (14) takes the form

$$\begin{aligned}
&\nu\frac{\partial\tilde{\chi}}{\partial\tau}+\frac{1}{\xi}\frac{\partial\chi_0}{\partial\xi}\left(\tilde{f}+\frac{\partial\tilde{f}}{\partial z}\right)+\frac{1}{\xi}\frac{\partial\tilde{\chi}}{\partial\xi}f_0\\
&-\frac{\chi_0}{\xi^2}\left(\tilde{f}-\xi\frac{\partial\tilde{f}}{\partial\xi}+\frac{\partial\tilde{f}}{\partial z}\right)-\frac{\tilde{\chi}}{\xi^2}\left(f_0-\xi\frac{\partial f_0}{\partial\xi}\right)\\
&-\frac{1}{\xi}\frac{\partial f_0}{\partial\xi}\left(-2\tilde{\chi}+\frac{\partial\tilde{\chi}}{\partial z}\right)+\frac{2\chi_0}{\xi}\frac{\partial\tilde{f}}{\partial\xi}\\
&+\nu\left(\frac{2}{\xi}\frac{\partial\tilde{f}}{\partial\tau}+2\frac{\partial^2\tilde{f}}{\partial\tau\partial\xi}-\frac{2}{\xi}\frac{\partial^2\tilde{f}}{\partial\tau\partial z}\right)\\
&=\nu\left(6\tilde{\chi}-4\frac{\partial\tilde{\chi}}{\partial z}+6\xi\frac{\partial\tilde{\chi}}{\partial\xi}-2\xi\frac{\partial^2\tilde{\chi}}{\partial z\partial\xi}\right.\\
&\left.+\xi^2\frac{\partial^2\tilde{\chi}}{\partial\xi^2}+\frac{\partial^2\tilde{\chi}}{\partial z^2}-\frac{\partial\tilde{\chi}}{\partial z}+\frac{\partial^2\tilde{\chi}}{\partial\xi^2}+\frac{1}{\xi}\frac{\partial\tilde{\chi}}{\partial\xi}-\frac{\tilde{\chi}}{\xi^2}\right),
\end{aligned}\tag{15}$$

$$\begin{aligned}
\tilde{\chi}&=\left(\frac{1}{\xi}+\xi\right)\frac{\partial^2\tilde{f}}{\partial\xi^2}+\frac{2}{\xi}\frac{\partial\tilde{f}}{\partial z}-2\frac{\partial^2\tilde{f}}{\partial z\partial\xi}\\
&+\frac{1}{\xi}\left(\frac{\partial^2\tilde{f}}{\partial z^2}-\frac{\partial\tilde{f}}{\partial z}\right)-\frac{1}{\xi^2}\frac{\partial\tilde{f}}{\partial\xi}.
\end{aligned}\tag{16}$$

The solution to the set of Eqs. (15) and (16) is sought in the form

$$\tilde{f}(\xi,z,\tau)=f_1(\xi)e^{\alpha z-i\omega\tau},\quad \tilde{\chi}(\xi,z,\tau)=\chi_1(\xi)e^{\alpha z-i\omega\tau}.\tag{17}$$

We obtain

$$\left(\xi+\frac{1}{\xi}\right)\frac{d^2f_1}{d\xi^2}-\left(2\alpha+\frac{1}{\xi}\right)\frac{df_1}{d\xi}+\frac{\alpha(\alpha+1)}{\xi}f_1=\chi_1,\tag{18}$$

$$\begin{aligned}
&\left(1+\xi^2\right)\frac{d^2\chi_1}{d\xi^2}+\left(6\xi-2\xi\alpha+\frac{1}{\xi}\right)\frac{d\chi_1}{d\xi}\\
&+\left(6-5\alpha+\alpha^2-\frac{1}{\xi^2}\right)\chi_1+i\omega\chi_1\\
&-\frac{\mathrm{Re}}{\varepsilon}\frac{f_0}{\xi}\frac{d\chi_1}{d\xi}+\frac{\mathrm{Re}}{\varepsilon}\frac{1}{\xi^2}\left(f_0-\xi\frac{df_0}{d\xi}\right)\chi_1\\
&+\frac{\mathrm{Re}}{\varepsilon}\frac{1}{\xi}\frac{df_0}{d\xi}(\alpha-2)\chi_1=\frac{\mathrm{Re}}{\varepsilon}\left(\frac{1}{\xi}(1+\alpha)\frac{d\chi_0}{d\xi}f_1-\frac{\chi_0}{\xi^2}\right.\\
&\left.\times\left((1+\alpha)f_1-\xi\frac{df_1}{d\xi}\right)+\frac{2}{\xi}\chi_0\frac{df_1}{d\xi}\right)\\
&+\frac{2i\omega}{\xi}(\alpha-1)f_1-2i\omega\frac{df_1}{d\xi}.
\end{aligned}\tag{19}$$

The boundary conditions for an axisymmetric mode follow from

(i) the equality of the radial velocity on the jet axis to zero,

$$u\big|_{r=0}=0\quad\text{or}\quad\frac{1}{\xi}\left(f_1(1+\alpha)-\xi\frac{df_1}{d\xi}\right)\Big|_{\xi=0}=0,\tag{20}$$

(ii) the equality of the tangential stress on the jet axis to zero,

$$\sigma_{rz}\big|_{r=0}=\left(\frac{\partial w}{\partial r}+\frac{\partial u}{\partial z}\right)\Big|_{r=0}=\left(2\frac{\partial w}{\partial r}+\Omega\right)\Big|_{r=0}=0\quad\text{or}\quad\chi_1\big|_{\xi=0}=0,\tag{21}$$

(iii) the condition of a decrease in perturbations of the average flow at infinity

$$f_1,\chi_1\big|_{\xi\to\infty}=0.\tag{22}$$

The set of Eqs. (18) and (19) with boundary conditions (10)–(22) at a fixed α represents a problem for the eigenfunctions f_1,χ_1 and the eigenvalue ω. For the numerical solution of the problem, it is convenient to introduce new variables

$$t=\xi^2,\quad\theta=\chi_1\xi,\quad\phi=f_1,$$

and notations

$$\phi_0=f_0,\quad\Phi_0=\frac{1}{\xi}\frac{df_0}{d\xi},\quad\theta_0=\frac{\chi_0}{\xi},\quad\Theta_0=\frac{d\chi_0}{d\xi}.\tag{23}$$

Then, the set of Eqs. (18) and (19) is written as

$$4(1+t)\frac{d^2\phi}{dt^2}+(2-4\alpha)\frac{d\phi}{dt}+\frac{\alpha(\alpha+1)}{t}\phi=\frac{\theta}{t},\tag{24}$$

$$\begin{aligned}
&\frac{d^2\theta}{dt^2}+\frac{(5-2\alpha)}{2(1+t)}\frac{d\theta}{dt}+\frac{(\alpha-2)(\alpha-1)}{4t(1+t)}\theta+\frac{i\omega}{4t(1+t)}\theta\\
&-\frac{\mathrm{Re}}{\varepsilon}\frac{\phi_0}{2t(1+t)}\left(\frac{d\theta}{dt}-\frac{\theta}{t}\right)+\frac{\mathrm{Re}}{\varepsilon}\frac{(\alpha-3)\Phi_0}{4t(1+t)}\theta\\
&=\frac{\mathrm{Re}}{\varepsilon}\left(\frac{(\alpha+1)(\Theta_0-\theta_0)}{4t(1+t)}\phi+\frac{3\theta_0}{2(1+t)}\frac{d\phi}{dt}\right)\\
&+\frac{i\omega}{2t(1+t)}(\alpha-1)\phi-\frac{i\omega}{(1+t)}\frac{d\phi}{dt},
\end{aligned}\tag{25}$$

and boundary conditions (20)–(22) take the form

$$\theta\big|_{t=0}=0,\quad\phi\big|_{t=0}=0,\tag{26}$$

$$\theta\big|_{t\to\infty}=0,\quad\phi\big|_{t\to\infty}=0;\tag{27}$$

in this case, $\theta'(0)\neq0$, $\phi'(0)\neq0$.

The algorithm for solving this problem is as follows. First, boundary problem (26)–(27) for determining θ_1, φ_1, θ_2, φ_2 satisfying the conditions for zero $\phi_1'(0)=1$, $\theta_1'(0)=\lambda_1$ and $\phi_2'(0)=1$, $\theta_2'(0)=\lambda_2$ is solved. In this case, an implicit finite-difference method based on the Gauss elimination is used to solve the set of linear equations obtained from the difference approximation of the set of Eqs. (24)–(25) [20]. The required solution represents the following linear combinations

$$\theta=A\theta_1+B\theta_2,\qquad\phi=A\phi_1+B\phi_2.\tag{28}$$

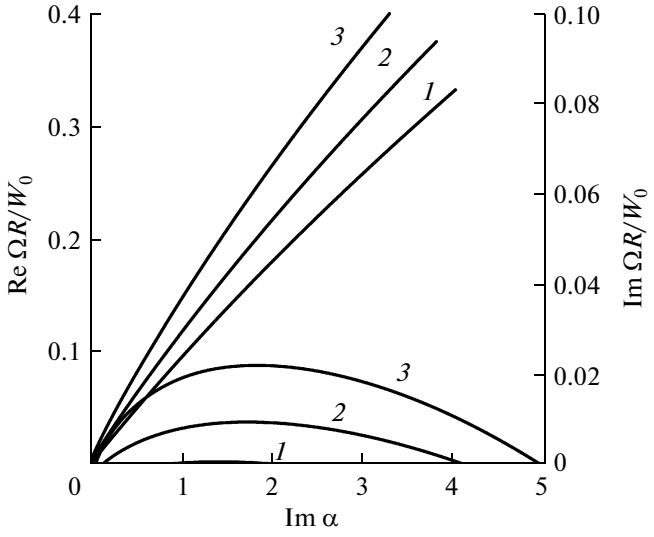

Fig. 4. Analogs of the dispersion curves at Re = 50: (*1*) ε = 0.08, (*2*) ε = 0.1, and (*3*) ε = 0.12.

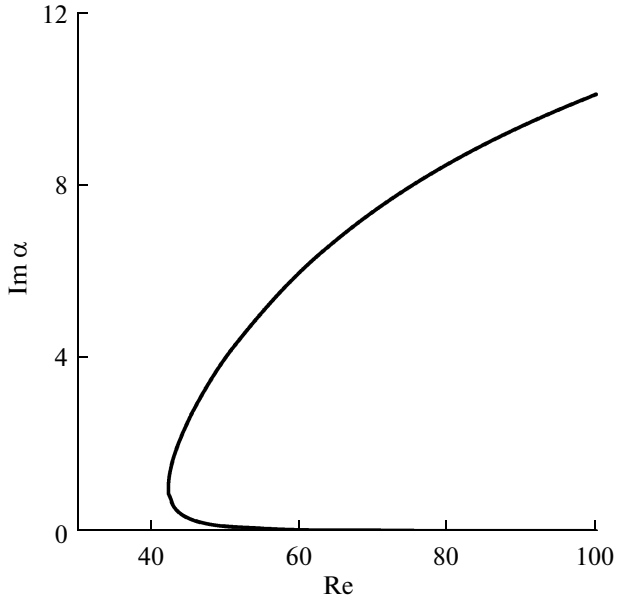

Fig. 5. The boundary of the stability region in the plane of the parameters (Re, Im α) at ε = 0.1.

Using conditions (28), we obtain the following equation to find the eigenvalue ω

$$\theta_1(0)\phi_2(0) - \theta_2(0)\phi_1(0) = 0. \quad (29)$$

The estimated Reynolds number, determined by molecular viscosity, is 6000 for the parameters of the experiment However, it can decrease by several orders of magnitude due to turbulent viscosity. The results of a calculation of the axisymmetric mode stability at the Reynolds number of 50 are presented in Fig. 4. It can be seen that at small convergence parameters the axisymmetric mode becomes stable, and the mode increment also increases with its growth. Figure 5 shows the boundary of the stability region in the plane of the parameters (Re, Im α) at ε = 0.1.

To understand the reason for the development of an unstable axisymmetric mode on a nonparallel flow, we consider the law of conservation of the kinetic energy $e = \frac{u_r^2 + u_x^2}{2}$ of a liquid particle in cylindrical coordinates in the form suggested in [2]:

$$\frac{\partial e}{\partial t} + U_r\frac{\partial e}{\partial r} + U_x\frac{\partial e}{\partial x} = \nu\Delta e + \mu_1 + \mu_2 + \mu_3, \quad (30)$$

where

$$\mu_1 = -u_x u_r\left(\frac{\partial U_r}{\partial x} + \frac{\partial U_x}{\partial r}\right) - u_r^2\frac{\partial U_r}{\partial r} - u_x^2\frac{\partial U_x}{\partial x}, \quad (31)$$

$$\mu_2 = -u_r\frac{\partial p}{\partial r} - u_x\frac{\partial p}{\partial x}, \quad (32)$$

$$\mu_3 = -\nu\left\{\left(\frac{\partial u_r}{\partial r}\right)^2 + \left(\frac{\partial u_r}{\partial x}\right)^2 + \left(\frac{\partial u_x}{\partial r}\right)^2 + \left(\frac{\partial u_x}{\partial x}\right)^2\right\}. \quad (33)$$

It follows from (30) that time variations in the liquid particle energy are related to

(1) diffusion described by the first term in the right-hand side,

(2) the energy transfer from the average flow to perturbations (31),

(3) losses of the kinetic energy for the transfer of the liquid particle from low- to high-pressure region (or the energy increment if otherwise) (32),

(4) viscous losses (33).

We focus on the last term in Eq. (31), which vanishes if the flow is plane-parallel. At $\frac{\partial U_x}{\partial x} < 0$, this term leads to an increase in the kinetic energy of the liquid particle. Thus, due to the nonparallelism of the flow (in particular, gue to the jet deceleration effect), an additional radiation force arises that is responsible for transferring the energy from the average flow to perturbations.

3. ESTIMATION OF THE AXISYMMETRIC MODE FREQUENCY FOR THE EXPERIMENTAL DATA. POSSIBILITIES OF A SELF-OSCILLATION REGIME OF THE AXISYMMETRIC MODE

Let us estimate the frequency of the varicose mode for the data of the experiment. Note that the eigenvalue ω is related to the physical frequency Ω by the relationship $\Omega = \frac{\omega\nu}{x^2}$. This means that the mode frequency depends on the distance along the jet. Let us estimate the frequency at the thermocline entrance for the parameters of the experiment. We normalize the

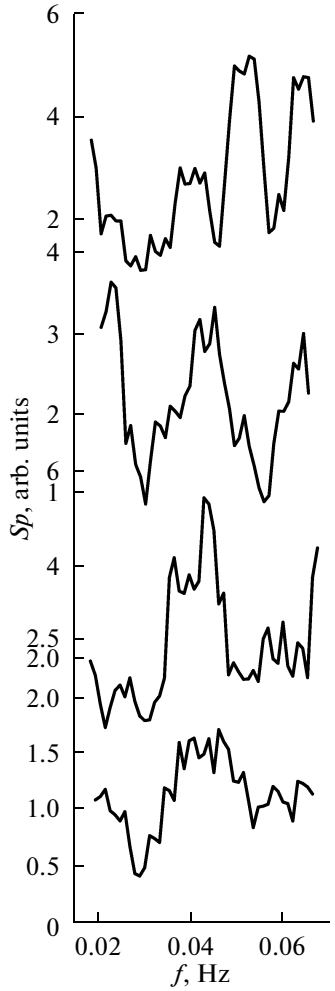

Fig. 6. The spectra of radius oscillations for four cross sections of the jet in the thermocline vicinity.

physical frequency to $\frac{W_0}{R_0}$; then, we have $\frac{\Omega}{W_0/R_0} = \omega\frac{\varepsilon^2}{\mathrm{Re}}$. The dispersion curves for Re = 50 are shown in Fig. 4. It can be seen that the mode with the dimensionless frequency of 0.22 will be the most unstable. According to the experimental data, near the thermocline, $\frac{W_0}{R_0} \approx 0.8–1.1\ \mathrm{s}^{-1}$. Then, the frequency of the most unstable mode is in the range of 0.028–0.039 Hz; i.e., it is close to the frequency of the peaks of the internal waves spectra (0.032–0.04 Hz).

On the other hand, it has been shown in Section 1 that the upper boundary of the jet also oscillates with a frequency close to the frequency of internal waves. The jet in the lower part of the thermocline and above the thermocline oscillates at one and the same frequency. This makes it possible to assume that an unstable global mode localized in the thermocline region and leading to a self-oscillation regime can develop on the jet. The underwater video recording makes it possible to study the spectra of oscillations of the axisymmetric mode in different cross sections along the jet (Fig. 6). It can be seen from the figure that the perturbation at a frequency close to 0.04 Hz is present in all spectra. This counts in favor of the assumption on the excitation of the global mode in this system [17].

It was shown in [17] that a necessary condition for an increase in the unstable global mode on the jet flow is its absolute instability in some finite region along the direction of the jet propagation. A counterflow on the average velocity profiles can serve as a reason for the development of the absolute instability of the plane-parallel and weakly nonparallel jet flow [17, 21]. The counterflow can be easily seen on the jet velocity profiles in the thermocline region (Fig. 7).

Let us qualitatively analyze the stability of the diverging flow, whose longitudinal velocity profiles coincide with the experimentally measured ones (see Fig. 7), where the divergence parameter is 0.35 and the Reynolds number is 300. The velocity profiles are approximated well by a function of the type

$$W/W_0 = a_1 e^{-a_2\xi^2/\varepsilon^2} + \left(a_3 e^{-a_4\xi^2/\varepsilon^2} - a_5\right)e^{-a_6\xi^6/\varepsilon^6},$$

where a_i, $i = \overline{1,6}$ are the constants (for the velocity profiles in Fig. 7 see the table).

Let us use the Briggs criterion [22, 23], according to which the instability will be absolute if the imaginary part of the absolute frequency is positive and will be convective if it is negative. The absolute frequency is determined from the condition of equality of the complex group velocity of the perturbation to zero $\frac{\partial\omega}{\partial k} = 0$ and it corresponds to the saddle point in the

Table

Profile no.	a_1	a_2	a_3	a_4	a_5	a_6
1	0.13	2.16	2.0	0.58	1.13	0.062
2	0.31	1.45	2.0	0.49	1.31	0.058
3	0.20	1.38	2.0	0.56	1.19	0.049
4	0.20	1.24	2.0	0.56	1.20	0.044
5	0.20	1.00	2.0	0.59	1.20	0.041
6	0.20	1.00	2.00	0.58	1.21	0.037

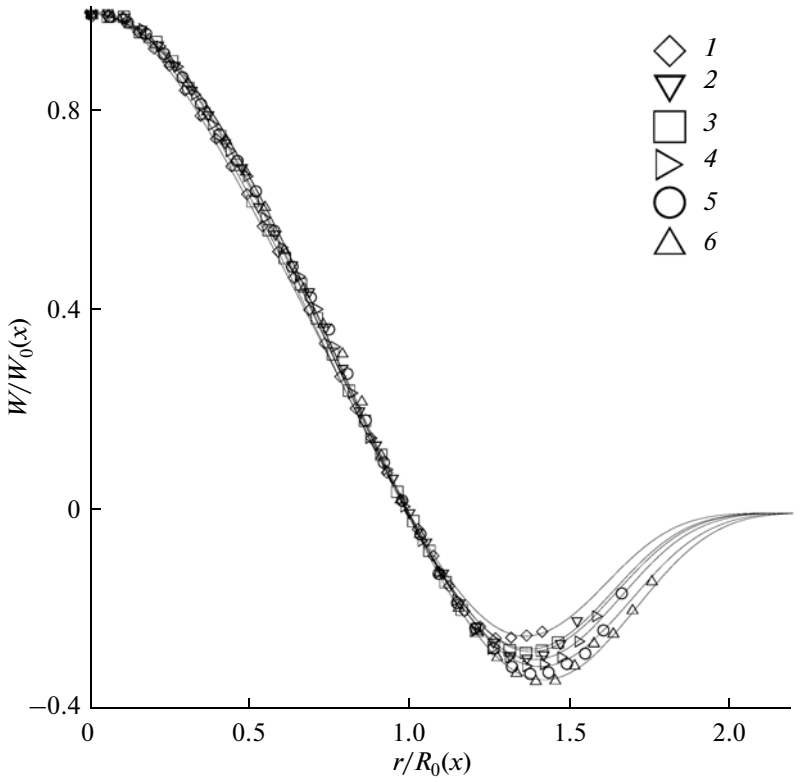

Fig. 7. Approximation of the profiles of the longitudinal jet velocity in the upper part of the thermocline. The least counterflow (*1*) corresponds to the velocity profile in the jet cross sections positioned at 1/4 of the thermocline depth upward from its center. The intensification of the counterflow corresponds to successive profiles (*2*)–(*6*), which are 1 cm apart along the jet propagation direction.

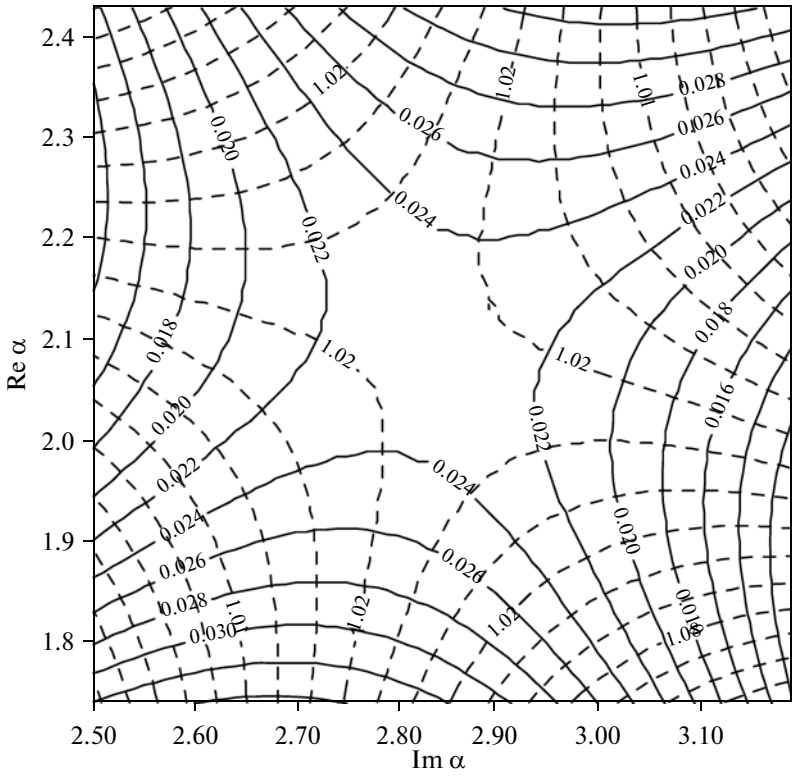

Fig. 8. The level curves of the real (dashed line) and imaginary (solid line) parts of the frequency on the $(\mathrm{Re}\,\alpha, \mathrm{Im}\,\alpha)$ plane.

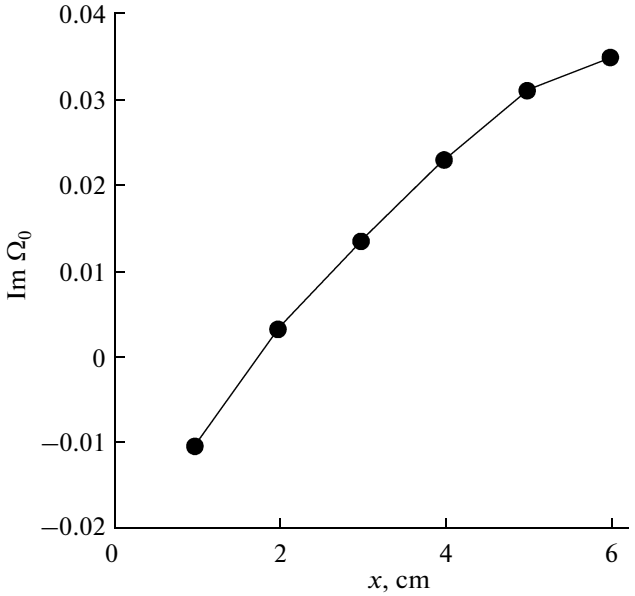

Fig. 9. The imaginary part of the absolute frequency as a function of distance from the longitudinal velocity profiles shown in Fig. 7.

complex plane of wavenumbers. For our problem, this condition takes the form $\frac{\partial\omega}{\partial\alpha} = 0$. Figure 8 shows the level curves of the real and imaginary parts of the frequency on the complex plane $(\mathrm{Re}\,\alpha, \mathrm{Im}\,\alpha)$ in the saddle-point vicinity for profile 3.

The dependence of the imaginary part of the absolute frequency for the longitudinal velocity profiles shown in Fig. 7 is plotted in Fig. 9. The minimal increment corresponds to velocity profile 1 with the least counterflow. It can be seen from the figure that the imaginary part of the absolute frequency becomes positive when the counterflow on the profiles of the jet longitudinal velocity intensifies. This means that the jet flow in the upper part of the thermocline is absolutely unstable. It was shown in [17] that the finite section of the absolute instability along the jet propagation direction is a necessary condition for the existence of the global mode. This condition is met for the flow in the upper part of the thermocline (see Fig. 9) and, thus, an unstable axisymmetric global mode can increase in this jet region, which confirms the conclusions on its excitation made experimental data.

CONCLUSIONS

The nonstationary dynamics of axisymmetric turbulent jets leading to the generation of internal waves was studied on the basis laboratory simulation at the LTST at the Institute of Applied Physics of the Russian Academy of Sciences. During the experiment, the jet in the thermocline was recorded using an underwater survey. Based on its results, the instantaneous velocity fields in the longitudinal jet cross section were measured using the PIV technique and the oscillations of the jet boundaries were analyzed. The simultaneous temperature measurements performed on different levels revealed intensive oscillations. A comparison of the internal wave spectra with the spectra of the jet oscillations in the thermocline region confirmed that the jet serves as a source of internal waves. Based on measured velocity data, we conducted a mode analysis of perturbations on the jet and showed that the axisymmetric mode is predominantly excited. The analysis of the hydrodynamic stability of the jet flow with a constant cross section and the velocity profiles simulating a flow near the thermocline showed that the axisymmetric mode is stable. The stability of the axisymmetric mode of the diverging jet flow with self-similar velocity profiles was studied. It was shown that the nonparallelism of the flow leads to instability of the axisymmetric mode. The estimated frequencies of the axisymmetric mode for the parameters corresponding to the conditions of the experiment are in agreement with the frequency of the maximum in the internal wave spectra. Based on an analysis of the experimental data, it was demonstrated that an axisymmetric mode is developed at one frequency (namely, the frequency of generation) in different cross sections of the jet in the thermocline vicinity, which points to the excitation of a globally unstable mode. This phenomenon was theoretically substantiated; in particular, it was shown that the counterflow on the profiles of the longitudinal jet velocity in the upper part of the thermocline causes the absolute instability of the flow required for the development of a global mode and the transition of the system to self-oscillations.

ACKNOWLEDGMENTS

This study was supported by the Ministry of Education and Science of the Russian Federation (Grant No. 16.518.11.7105) the Government of the Russian Federation (contract no. 34.31.0048), Russian Foundation for Basic Research, project nos. 09-05-00779-a, 11-05-00455-a, 12-05-00822-a and GFEN_a 10-05-91177, and the Federal Target Program "Scientific and Scientific–Pedagogical Personnel of Innovative Russia" for 2009–2013.

REFERENCES

1. G. K. Batchelor and A. E. Gill, "Analysis of the Stability of Axisymmetric Jets," J. Fluid Mech. **14** (4), 529–551 (1962).
2. R. Betchov and W. O. Criminale, Jr., *Stability of Parallel Flows* (Academic, New York–London, 1967).
3. A. Michalke, "Survey on Jet Instability Theory," Prog. Aerosp. Sci **22** (3), 159–199 (1984).
4. S. C. Crow and F. H. Champagne, "Orderly Structure in Jet Turbulence," J. Fluid Mech. **48** (3), 547–591 (1971).

5. M. Lessen and P. J. Singh, "The Stability of Axisymmetric Free Shear Flows," J. Fluid Mech. **60**, 433–457 (1973).
6. G. E. Mattingly and C. C. Chang, "Unstable Waves on an Axisymmetric Jet Column," J. Fluid Mech. **65**, 541–560 (1974).
7. P. Plaschko, "Helical Instabilities of Slowly Divergent Jets," J. Fluid Mech. **92**, 209–215 (1978).
8. A. Michalke and G. Hermann, "On the Inviscid Instability of a Circular Jet with External Flow," J. Fluid Mech. **114**, 343–359 (1982).
9. M. Yoda, L. Hesselink, and M. D. Mungal, "The Evolution and Nature of Large-Scale Structures in the Turbulent Jet," Phys. Fluids A **4** (4), 803–811 (1992).
10. A. Agrawal and A. K. Prasad, "Organisational Modes of Large-Scale Vortices in an Axisymmetric Turbulent Jet," Flow, Turbul. Combust. **68** (4), 359–377 (2002).
11. P. E. Dimotakis, R. C. Miake-Lye, and D. A. Papantoniou, "Structure and Dynamics of Round Turbulent Jets," Phys. Fluids **26** (11), 3185–3192 (1983).
12. S. Gamard, D. Jung, and W. K. George, "Downstream Evolution of the Most Energetic Modes in a Turbulent Axisymmetric Jet at High Reynolds Number. Part 2. The Far-Field Region," J. Fluid Mech. **514**, 205–230 (2004).
13. E. V. Ezhova, D. A. Sergeev, A. A. Kandaurov, et al., "Nonstationary Dynamics of Submerged Turbulent Axisymmetric Jets in a Stratified Fluid. Part 1: Experimental Study," Izv., Atmos. Ocean. Phys. **48** (4), 461–470 (2009).
14. *Theory of Turbulent Jets*, Ed. by G. N. Abramovich (Nauka, Moscow, 1984) [in Russian].
15. V. Shtern and F. Hussain, "Effect of Deceleration on Jet Instability," J. Fluid Mech. **480**, 283–309 (2003).
16. P. A. Monkewitz, "The Absolute and Convective Nature of Instability in Two-Dimensional Wakes at Low Reynolds Numbers," Phys. Fluids **31**, 999–1006 (1988).
17. P. Huerre and P. A. Monkewitz, "Local and Global Instabilities in Spatially Developing Flows," Annu. Rev. Fluid Mech. **22**, 473–537 (1990).
18. K. K. Tam, "Linear Stability of the Non-Parallel Bickley Jet," Can. Appl. Math. Quart. **3**, 99–110 (1996).
19. A. McAlpine and P. G. Drazin, "On the Spatio-Temporal Development of Small Perturbations of Jeffery–Hamel Flows," Fluid Dyn. Res. **22** (3), 123–138 (1998).
20. Yu. I. Troitskaya, "Viscous-Diffusion Nonlinear Critical Layer in a Stratified Shear Flow," J. Fluid Mech. **233**, 25–48 (1991).
21. P. A. Monkewitz, P. Huerre, and J.-M. Chomaz, "Global Linear Stability Analysis of Weakly Non-Parallel Shear Flows," J. Fluid Mech. **251**, 1–20 (1993).
22. R. J. Briggs, *Electron-Stream Interaction with Plasmas* (Cambridge, Mass., MIT Press, 1964).
23. *Fundamentals of Plasma Physics*, Ed. by A. A. Galeev and R. Sudan (Energoatomizdat, Moscow, 1984), Vol. 2 [in Russian].